Original

Deng, Q.; Gosslar, D.-H.; Smetanin, M.; Weissmueller, J.:
Electrocapillary coupling at rough surfaces
In: Physical Chemistry Chemical Physics (2015) Royal Society of Chemistry

DOI: 10.1039/c5cp00167f

PCCP

PAPER

View Article Online
View Journal | View Issue

Cite this: *Phys. Chem. Chem. Phys.*, 2015, **17**, 11725

Received 12th January 2015,
Accepted 27th March 2015

DOI: 10.1039/c5cp00167f

www.rsc.org/pccp

Electrocapillary coupling at rough surfaces

Qibo Deng,*[a] Daniel-Hendrik Gosslar,[a] Maxim Smetanin[b] and Jörg Weissmüller[ac]

We investigate the impact of the surface roughness on the experimental value of the electrocapillary coupling coefficient, ς. This quantity relates the response of electrode potential, E, to tangential elastic strain, e, and also measures the variation of the surface stress, f, with the superficial charge density, q. We combine experiments measuring the apparent coupling coefficient ς_{eff} for gold thin film electrodes in weakly adsorbing electrolyte with data for the surface roughness determined by atomic force microscopy and by the capacitance ratio method. We find that even moderate roughness has a strong impact on the value of ς_{eff}. Analyzing the mechanics of corrugated surfaces affords a correction scheme yielding values of ς that are invariant with roughness and that agree with expectations for the true coupling coefficient on ideal, planar surfaces. The correction is simple and readily applied to experiments measuring ς_{eff} from surface stress changes in cantilever bending studies or from the potential variation in dynamic electro-chemo-mechanical analysis.

I. Introduction

The recent past has seen an increasing interest in the coupling between surface mechanics and electrode processes. This electrocapillary coupling is significant for the surface electronic structure[1–3] and for the charge transfer during electrosorption.[4,5] Electrocapillary coupling is also intricately connected to catalysis with strained layers, a current issue in modeling[6–8] and experiment.[9–12] It has been shown that the electrocapillary coupling parameters measure the variation of the adsorption enthalpies and barrier heights with strain.[13–15] This is significant since it opens a way towards the experimental quantification of the physical phenomena that underly the enhanced performance of strained-layer catalysts. That notion is indeed supported by experiments probing the mechanical modulation of electrocatalytic reactivity *in situ* during straining and by the excellent agreement of the results with kinetic rate equations embodying the experimental coupling parameters.[14] For a current review on electrocapillary coupling see ref. 16.

The electrocapillary coupling is measured by the parameter, ς, which quantifies the variation of the electrode potential, E, with tangential strain, e. A Maxwell relation[17,18] equates ς for any given electrode process to the respective variation of a capillary force, the surface stress f, with superficial charge density q. Thus, one has

$$\varsigma = \mathrm{d}E/\mathrm{d}e|_q = \mathrm{d}f/\mathrm{d}q|_e . \quad (1)$$

This implies that electrocapillary coupling can be equivalently measured in two seemingly independent ways, namely from the variation of the surface stress with charge density at constant strain or from the variation of the electrode potential with strain at constant charge density. The first approach can be implemented by cantilever bending experiments[19–21] or porous metal dilatometry,[22–24] while the second requires experiments which cyclically strain a planar electrode simultaneously with electrochemical characterization.[15,25] The numerical values of ς emerging from the respective approaches are found in excellent agreement.[15,16,19,20,22,25]

Besides the relevance of the above experiments for the physics of adsorption and for catalysis, cantilever bending is also of technological relevance for various sensing schemes, such as DNA detection and analysis.[26] In view of the significance of experiments probing the variation of surface stress on planar surfaces during electric charging or adsorption and of the complementary experiments measuring the variation of the electrode potential with strain, it is significant that real surface are never perfectly planar and that experiment points at a strong impact of surface corrugation on the experimental phenomena. In fact, several studies reported the effect of surface roughness or of deliberately introduced nanoscale surface corrugation on the apparent variation in surface stress.[27–31] For instance, Tabard-Cossa found that the cantilever bending amplitude during the potential-induced anion adsorption varied by up to a factor of three when the surface relief was varied.[31] This raises the question, how reliable are experimental values for the surface stress and

[a] *Institut für Werkstoffphysik und Werkstofftechnologie, Technische Universität Hamburg-Harburg, Hamburg, Germany. E-mail: Qibo.Deng@tuhh.de*
[b] *Department of Chemistry, University of Guelph, Guelph, Canada*
[c] *Institut für Werkstoffforschung, Werkstofmechanik, Helmholtz-Zentrum Geesthacht, Geesthacht, Germany*

for the electrocapillary coupling, given the inevitable deviation from surface planarity? In this work, we discuss this issue and we explore a strategy for correcting the impact of roughness.

Our approach rests on theory analyzing the impact of surface corrugation on the way in which the surface stress is transferred into the underlying bulk solid.[32,33] Typically, roughness reduces the effective action of the surface stress on the bulk, to the extent that the effective stress which is coupled into the solid can even invert its sign.[32]

Since electrocapillary coupling is inherently related to the surface stress, the observations on the impact of roughness on surface stress imply that roughness will also affect the measurement of electrocapillary coupling parameters ς. Here, we present an analysis of that issue combining theory and experiment. For the limiting case of not too large roughness we derive simple correction scheme that works with experimentally accessible measures for surface roughness and that afford a significantly enhanced accuracy of the data for ς.

II. Theory

A. Parameterizing roughness

Our description of surface roughness (Fig. 1) is based on the notions of a planar (idealized, macroscopic) surface S and of a microscopically corrugated surface, $\hat{S}$, with surface height profile $h(\mathbf{r})$ (the local height of $\hat{S}$ over S at position vector $\mathbf{r}$) that takes the form of a continuously differentiable but otherwise arbitrary function of $\mathbf{r}$. At any position $\mathbf{r}$, the inclination of the surface is measured by the angle $\theta(\mathbf{r})$, that is, the angle included by the normal, $\mathbf{n}$, of S and the local normal, $\hat{\mathbf{n}}$, of $\hat{S}$.

In experiment, surface area is readily quantified by various techniques, and it is of interest to explore roughness parameters that depend on the area. As an example for such a parameter, the "roughness factor", ρ, is defined as the ratio between actual, $\hat{A}$, and projected (apparent macroscopic) surface areas, A_{eff}, in other words,

$$\rho = \hat{A}/A_{\mathrm{eff}}. \tag{2}$$

The height profile $h(\mathbf{r})$ is also accessible to the experiment, *e.g.* measuring a surface topography by atomic force microscopy (AFM). Based on the function $h(\mathbf{r})$ one can compute the inclination angle $\theta(\mathbf{r})$, and it turns out that this function provides an independent approach toward the roughness factor. In the limiting case of not too large θ one finds a good approximation in our previous work.[32,33]

$$\rho \approx 1 + \frac{1}{2}\langle\theta^2\rangle, \tag{3}$$

where the brackets denote averaging over positions on the surface S.

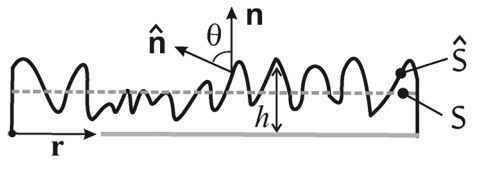

Fig. 1 Schematic display of a microscopically corrugated surface $\hat{S}$ with surface height profile $h(\mathbf{r})$ at position vector $\mathbf{r}$. S: a planar (idealized, macroscopic) surface. The inclination angle of the surface θ is included by the normal, $\mathbf{n}$, of S and the local normal, $\hat{\mathbf{n}}$, of $\hat{S}$. Adapted from ref. 32.

B. Impact of roughness on measurement of surface stress

In general, the corrugation of a surface may be anisotropic (as, for instance, in a corrugated-sheet type structure with parallel ridges and valleys) and the effective surface stress will then also be anisotropic. In the interest of conciseness, we here ignore this anisotropy and assume that the surface profile is macroscopically isotropic.

Furthermore, we assume that the local surface stress, $\hat{\mathbf{s}}$, on $\hat{S}$ is isotropic, so that the local and the effective macroscopic surface stresses may both be represented by scalar quantities, which we denote by $\hat{f}(\mathbf{r})$ and by f_{eff}, respectively. In terms of the surface projection tensor, $\hat{\mathbf{P}}$,[34] on $\hat{S}$ the local surface stress here obeys $\hat{\mathbf{s}}(\mathbf{r}) = \hat{f}(\mathbf{r})\hat{\mathbf{P}}(\mathbf{r})$. It is important to note that f_{eff} describes the effective (or apparent) surface stress that is accessible to the experiment, *e.g.* by cantilever bending. We emphasize that both $\hat{\mathbf{s}}$ on $\hat{S}$ and $\hat{\mathbf{s}}_{\mathrm{eff}}$ on S are isotropic in the plane. Therefore, the scalar surface stress magnitude f and f_{eff} contain the full information on surface stress on any surface of known orientation. As a consequence, f or f_{eff} is the appropriate thermodynamic parameter and eqn (1) applies.

Irrespective of the anisotropy, the roughness of a surfaces affects the coupling of the surface stress into the underlying bulk through three factors, namely (1) the increase in surface area, (2) the fact that the surface stresses, being tangential in local surface coordinates,[34] act under an angle to the macroscopic surface plane, and (3) the presence of an out-of-plane stress component near the surface, which couples into the in-plane stress due to the elastic transverse response. As has been discussed in our previous work,[32,33] the increase in surface area tends to enhance the action of the surface stress, while the inclination and the transverse response reduce this action.

For an isotropic surface, and in the limit of not too large roughness (see below), the above mechanisms are embodied in a simple relation[32,33] between the local and effective surface stresses, the surface inclination and the Poisson ratio, ν, namely

$$f_{\mathrm{eff}} = \hat{f}\left[1 - \frac{\nu}{1-\nu}\langle\theta^2\rangle\right]. \tag{4}$$

By solving eqn (3) for θ^2 and inserting into the above equation, the result can be re-expressed in terms of the roughness factor as

$$f_{\mathrm{eff}} = \hat{f}\frac{1+\nu-2\nu\rho}{1-\nu}, \tag{5}$$

or equivalently

$$f_{\mathrm{eff}} = \hat{f}\left(1 - \frac{2\nu}{1-\nu}\Delta\rho\right) \tag{6}$$

with $\Delta\rho = \rho - 1$. Eqn (4) and (5) link the effective experimental signature of surface stress to the local, true value of the surface

stress and to the measures for the roughness and for the elastic transverse response of the material near the surface.

C. Impact of roughness on electrocapillary coupling strength

Measuring the electrocapillary coupling strength means quantifying the change in surface stress with superficial charge density, q. Similar to the surface stress, the effective macroscopic value of q will also differ from the local, true value whenever there is corrugation. Specifically, the effective charge density q_{eff} is measured as the net charge, Q, over the macroscopic, projected area, A_{eff}, of the surface. Taking into account the definition of the roughness factor (eqn (2)), q_{eff} can be linked to the true local charge density $\hat{q}$ via

$$q_{\mathrm{eff}} = \frac{Q}{A_{\mathrm{eff}}} = \rho\frac{Q}{\hat{A}} = \rho\hat{q}. \tag{7}$$

By means of the above equations for f_{eff} and q_{eff} we are now in a position to discuss the experimental value, ς_{eff} of the electrocapillary coupling parameter. Consistent with its definition through eqn (1), the experimental coupling parameter is determined as the derivative of effective surface stress with respect to effective superficial charge density. It is readily found that

$$\varsigma_{\mathrm{eff}} = \frac{\mathrm{d}f_{\mathrm{eff}}}{\mathrm{d}q_{\mathrm{eff}}} = \frac{\mathrm{d}\hat{f}}{\mathrm{d}\hat{q}}\frac{1+\nu-2\nu\rho}{(1-\nu)\rho} = \hat{\varsigma}\frac{1+\nu-2\nu\rho}{(1-\nu)\rho}, \tag{8}$$

where the parameter $\hat{\varsigma}$ denotes the true local value of the coupling coefficient. It is important to note that the Maxwell relation eqn (1) implies that eqn (8) applies equally to experiments measuring ς as the strain-derivative of the electrode potential at constant charge density:

$$\varsigma_{\mathrm{eff}} = \frac{\mathrm{d}E}{\mathrm{d}e}\Big|_{\mathrm{eff}} = \frac{\mathrm{d}f_{\mathrm{eff}}}{\mathrm{d}q_{\mathrm{eff}}} = \hat{\varsigma}\frac{1+\nu-2\nu\rho}{(1-\nu)\rho}. \tag{9}$$

Eqn (8) and (9) suggests that the surface roughness in the form of ρ significantly affects the apparent value of the potential–strain coefficient in dynamic electro-chemo-mechanical analysis (DECMA) experiment and the surface stress–charge density coefficient in cantilever wafer bending measurement. Experiments measuring ς_{eff} on nominally planar surfaces thus require a correction when the electrode surface is rough. The true value of electrocapillary coupling coefficient $\hat{\varsigma}$ is then given by

$$\hat{\varsigma} = \varsigma_{\mathrm{eff}}\frac{(1-\nu)\rho}{1+\nu-2\nu\rho}. \tag{10}$$

When expanding eqn (10) as a series in $\Delta\rho$, the leading term scales with $(1+\nu)/(1-\nu)$, which shows that the magnitude of the correction is larger for larger values of ν.

We have explored the validity of the ''small-roughness'' approximation by comparing the present equations to the more accurate results in ref. 32. For the Poisson ratio of Au we find that the correction is accurate to within 10% provided that the roughness factor does not exceed 1.25.

III. Experimental procedures

The procedures of this study are largely identical to those of our earlier report on dynamic electro-chemo-mechanical analysis (DECMA) on polarizable electrodes; see details in ref. 25. In the interest of a self-contained description, we present a brief display of the procedures.

The working electrodes (WE) are 50 nm thin gold films, sputtered onto 125 μm thick polyimide substrates (Upilex, UBE). After deposition, the film is annealed for 1 hour in vacuum of 10^{-6} mbar at 300 °C. All potentials in this work are quoted *versus* the standard hydrogen electrode (SHE) and are positive by 197 mV compared to potentials measured *versus* Ag/AgCl in 3.5 M KCl (World Precision Instruments). The electrolytes are prepared from $HClO_4$ (Suprapur, Merck) and ultra-pure water (18.1 MΩ cm, Sartotius), and deaerated with 99.9999% Ar gas. The glass electrochemical cell is placed into Piranha solution (5 volume parts of concentrated H_2SO_2 + 1 part of 30% H_2O_2) for 24 hours and then rinsed thoroughly with ultrapure water.

DECMA uses a lock-in amplifier to detect the potential modulation when the electrode is subjected to cyclic strains. A piezo actuator (PI-840 Physik Instrumente), fed by a function generator, imposes a sinusoidal cyclic elastic strain on the polyimide substrate of the WE. The grip displacement at any given time is read from the sensor in the piezo actuator and is used as the reference signal in the lock-in amplifier (SR 7270, Signal Recovery). We use a strain frequency of 20 Hz with an amplitude of $\sim 2 \times 10^{-4}$ in this study.

In situ magnetization and diffraction experiments under load have established that the substrate deformation is precisely transferred to the electrode when the surface is smooth.[35,36] With attention to experiments at small strains (amplitudes range from 10^{-4} to 10^{-3}), DECMA experiments for probing the electrocapillary coupling parameter ς can take the in-plane strain of the electrode layer equal to the applied strain on the polyimide substrate.[14,15,25]

Atomic force microscopy (STM5500, Agilent) in AC mode is used to characterize surface topology of the electrodes in this study.

IV. Results and discussion

A. Characterization

All experiments of this work used thin-film gold electrodes sputtered unto polyimide substrates and investigated in 10 mM $HClO_4$. Fig. 2 shows an exemplary cyclic voltammogram (CV) under these conditions. The data is consistent with CVs of clean gold surfaces of polycrystalline thin film metal electrode, see *e.g.* ref. 37 and 38.

Atomic force microscopy (AFM) characterizes the surface roughness properties of the as-prepared and annealed gold thin films. Typical AFM top-view amplitude images of these two different surface states are shown in Fig. 3(a) and (b), respectively. The height image representing the surface topography is recorded *in situ* with amplitude images. The surface topographies are

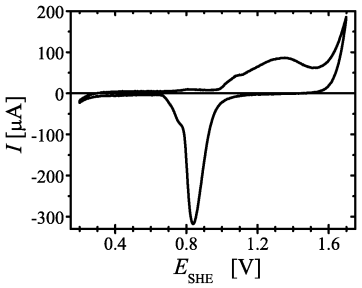

Fig. 2 Cyclic voltammogram of annealed gold electrode in 10 mM $HClO_4$ at a scan rate of 100 mV s^{-1}.

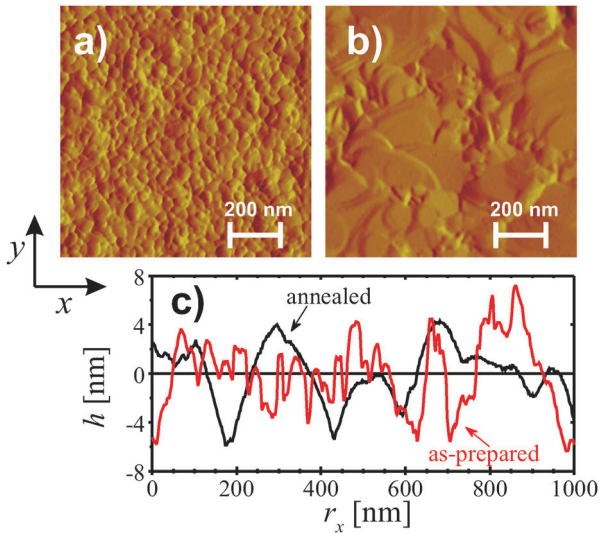

Fig. 3 A typical AFM top-view image of an electrode surface topography. Images of 1 μm × 1 μm area with 512 × 512 points: (a) of the as-prepared gold and (b) of the annealed gold thin films; (c) the corresponding topography cross sections.

recorded over scanned areas of 1 μm × 1 μm on several randomly chosen locations. The images are taken at a scan rate of 2 μm s^{-1} over the randomly selected areas. Fig. 3(c) shows exemplary height profiles for as-prepared and annealed electrodes. The mean slope is seen to lessen after annealing, demonstrating that this treatment smoothens the surface.

Our study used two independent approaches for determining the roughness factor. The first approach uses surface inclination angles based on AFM data. Note that AFM images are usually recorded as line scans along one axis – which we refer to as the *x*-axis – which are then concatenated to form a two-dimensional image. The scanning speed in the scan direction is then considerably higher than that in the orthogonal direction. As a result, the statistical properties of AFM data are usually collected along the *x* profiles (fast axis) as these are less affected by low frequency noise and thermal drift.[39,40]

The inclination angle, θ, at any position in an AFM height image can be derived from the one-dimensional tangent function of the surface along the fast scan axis. This uses $\theta = \arctan(\delta h/\delta x)$. The δ refer to the differences in height and in *x*-position between neighboring pixels. We evaluated a map of θ in this way by means of an algebra program (Mathematica). Averaging over the map provides the mean-square inclination $\langle\theta^2\rangle$ that yield the roughness factor through eqn (3). By applying the above technique to AFM data for as-prepared and annealed films, we can monitor the roughness factor in the initial and in the thermally treated state. For the as-prepared films this yields $\rho = 1.077 \pm 0.015$, while the value is $\rho = 1.014 \pm 0.011$ for the annealed surface. The calculated values of roughness factor exhibit a moderate difference for these two states. Inserting above values of ρ into eqn (9), the result suggests that the apparent experimental value of ς_{eff} is only 82% of the true coefficient value, $\hat{\varsigma}$, on this as-prepared surface while the apparent value approaches to 96% of $\hat{\varsigma}_{eff}$ on annealed surface. This demonstrates that even moderate roughness can have a strong impact on ς_{eff}. The DECMA measurement of ς_{eff} will be conducted with two different states to verify this expectation (see below).

The second approach for the determination of ρ uses the capacitance ratio method to determine the true surface area.[23,43] This method has the benefit of being applicable *in situ* in electrolyte although it is less direct than the AFM evaluation. The method thus affords monitoring the evolution of roughness, see below. The true surface area $\hat{A}$ is here determined by dividing the capacity, *C*, of the electrode by the capacitance (capacity per area), *c*, of the planar gold surface. In order to minimize the contributions of charge-transfer reactions, the evaluation exploits a narrow potential interval ($\sim$50 mV) within the capacitive region of the CV. Fig. 4(a) shows capacity data for the example of an electrode that was smoothed by thermal annealing treatment at the temperature of 300 °C for 1 h. The absence of transport limitations is evidenced by the fact that the average (over the anodic and cathodic branches) current magnitude at the center of the potential interval scales with the scan rate (Fig. 4(b)). The capacity is given by the slope of the graph of current *versus* scan rate; linear regression in the example suggests $C = 26.2 \pm 1.4$ μF on the annealed Au electrode with macroscopic surface area 0.55 cm^2 and roughness factor 1.014 (see AFM data above). The capacitance value of planar Au is thus given as 47 ± 3 μF cm^{-2}. This value is also consistent with the value of 45 μF cm^{-2} by the electrochemical impedance measurement.[25]

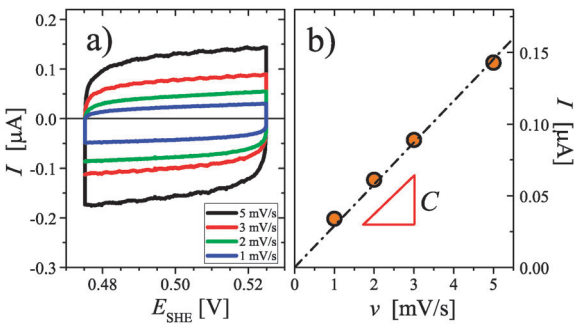

Fig. 4 (a) Cyclic voltammograms of rough electrode in small potential ranges (*ca.* 50 mV) at different scan rates (*v*) in 10 mM $HClO_4$ and (b) the slope of the average of absolute currents at the center of the potential interval *versus* the scan rate.

B. Electrocapillary coupling coefficient

We now turn the attention to DECMA experiments measuring the effective coupling parameter with as-prepared and annealed gold samples. As the two states exhibit different roughness, it is of interest to inspect the ramifications for the effective values of the electrocapillary coupling parameters. DECMA results were obtained under identical conditions, *i.e.*, 10 mM concentration solution of $HClO_4$, the cyclic strain frequency of 20 Hz and an amplitude of $e_0 = 2 \times 10^{-4}$. Fig. 5(a) displays the results. It is seen that the graphs of $\varsigma_{eff}(E)$ for both states exhibit qualitatively identical features, in good qualitative agreement with previous results in ref. 25. Yet, the two graphs are significantly shifted relative to each other along the ordinate.

Of particular interest is the value of the coupling parameter at the minimum of the $\varsigma_{eff}(E)$ graph. This corresponds to the maximum magnitude of the coefficient, which we find at $\sim$0.54 V, near the potential of zero charge (pzc).[25] The electrocapillary coupling coefficient near the pzc is of interest because it may be discussed relative to computations of the same parameter by *ab initio* density functional theory.[41,42] The data of Fig. 5(a), when taken at face value, suggest distinctly different values of the coupling parameter at the pzc depending on the roughness. The value of -1.59 ± 0.01 V for the rougher, as-prepared electrode compares to -1.86 ± 0.04 V for the annealed surface. Thus, the present experiments exemplify a significant dependency of the effective experimental electrocapillary coupling parameter on the roughness.

In situ uniaxial tensile testing and X-ray diffraction experiments[44] have determined the value of Poisson's ratio ν as 0.421 for gold thin films deposited on polyimide substrates, similar to our samples. We insert this Poisson's ratio of the gold thin film and the value of roughness factor calculated above from AFM data into the correction equation (eqn (10)). We have applied to the correction embodied by eqn (10) to the electrocapillary coupling coefficients of Fig. 5(a). Fig. 5(b) shows the results. It is seen, that the corrected data obtained from the experiments with the samples of different surface roughness now superimpose and thereby agree on the magnitude of the electrocapillary coupling. At -1.92 ± 0.01 V and -1.92 ± 0.04 V, respectively, the extremum values for as prepared and annealed gold films now agree within error bars. Overall, the large variation in apparent electrocapillary response and the good agreement achieved after correction support our theory of the impact of roughness on experiments in electrocapillarity.

The corrected coefficient value of $\hat{\varsigma}$ in this study is yielded as -1.92 ± 0.04 V near the pzc, which is supported by the computation value of -1.86 V on Au(111) single crystal surface by the density functional theory calculation.[41]

C. Roughness decay under applied potential conditions

As an independent verification of our approach we have roughened an electrode surface by an oxidation–reduction cycle and then studied, *in situ*, the evolution of the apparent electrocapillary coupling parameter as the roughness decayed with time.

In situ scanning tunneling microscopy[45,46] has revealed the roughening of Au surfaces after electrochemical oxidation and reduction, specifically when the maximum potential is high enough to cause a replacement-turnover process. The roughness decays spontaneously under either open circuit or applied potential conditions.[47–49] Here we applied a potential of 1.4 V for 25 minutes. The reduction is then achieved by a potential step at $E = 0.54$ V. The capacity data are recorded *in situ* in the same cell and immediately preceding the cyclic strain experiments, but with the strain switched off.

Fig. 6 shows the transient of the capacity during the recovery. The decay of C monitors the smoothing of the surface. For use with the capacity data, the definition of ρ in eqn (2) can be rewritten as

$$\rho = \frac{\hat{A}}{A_{eff}} = \frac{C}{cA_{eff}}, \qquad (11)$$

where the capacity C is given in Fig. 6(b). The macroscopic projected surface area is determined by analyzing the footprint of the meniscus on the sample after experiment, $A_{eff} = 0.8 \pm 0.05$ cm^{-2}. The roughness factor was obtained by evaluating eqn (11) with the true capacitance, $c = 47$ mF cm^{-2} and the result

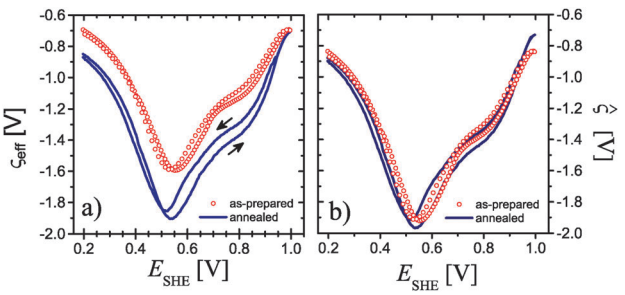

Fig. 5 Impact of roughness for the electrocapillary coupling coefficient ς. (a) Experimental ("effective") coupling coefficient, ς_{eff}, for as-prepared (circles) and annealed (lines) electrodes *versus* electrode potential, E. Measurement by dynamic electro-chemo-mechanical analysis in 10 mM $HClO_4$, potential scan rate 1 mV s^{-1} and strain frequency 20 Hz. Arrows indicate sweep direction. (b) True value of local coupling coefficient, $\hat{\varsigma}$, as estimated from the data in (a) by applying the correction of eqn (10).

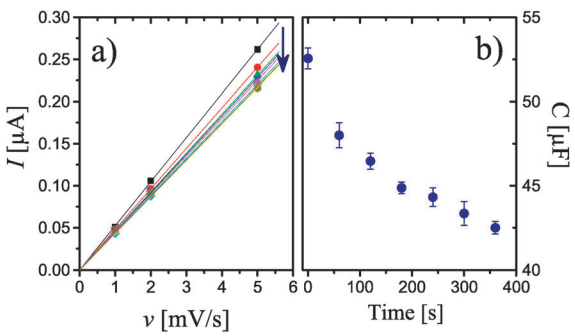

Fig. 6 Exploring the time-dependence of capacity, C, at $E = 0.54$ V during the recovery of the surface after roughening by oxygen species desorption. Part (a): average magnitude, I, of current *versus* potential scan rate, v, at different times after desorption. Arrow denotes sequence of subsequent measurements. Part (b): time-dependence of C as inferred from data in part (a).

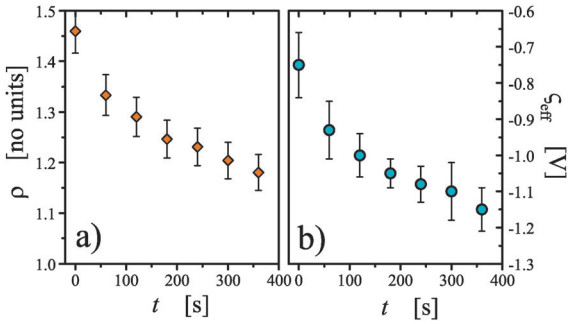

Fig. 7 Time-dependence of roughness factor, ρ, and of the effective electrocapillary coupling parameter, ς_{eff}, at E = 0.54 V during the recovery of the surface after roughening by oxygen species desorption. Note the large deviation from the true value of ς.

is shown in Fig. 7(a). It can be seen that ρ starts out as large as $\sim$1.5. It is also seen that the surface smoothes with a characteristic time in the order of minutes, in agreement with data in ref. 45. After around 360 s the roughness attains a nearly stationary value.

Fig. 7(b) shows the values of the apparent electrocapillary coupling coefficient measured during the evolution from very rough to smooth the surface. At −0.75 V, the experiment initially finds only about 40% of the corrected value obtained for the annealed gold film. While the surface smoothens, the coefficient increases in magnitude. Yet, as the roughness remains finite, ς_{eff} does not approximate the true value of the coupling coefficient.

Since our analysis in Section IIC implies that eqn (10) is no longer a good approximation when the roughness exceeds 1.25, we refrain from applying the correction here. Yet, it is still of interest to compare the roughness-imposed variation of the effective electrocapillary coupling coefficient near the pzc to the prediction by eqn (10). This comparison is shown in Fig. 8. Inspecting first the ς_{eff} from the annealing experiment (circles in the figure), it is seen that this data agrees precisely with the prediction. The data from the relaxation experiment do also agree with the prediction as long as the value of ρ does not significantly exceed 1.2. For larger roughness factors, eqn (10) overestimates the actual variation in ς_{eff}.

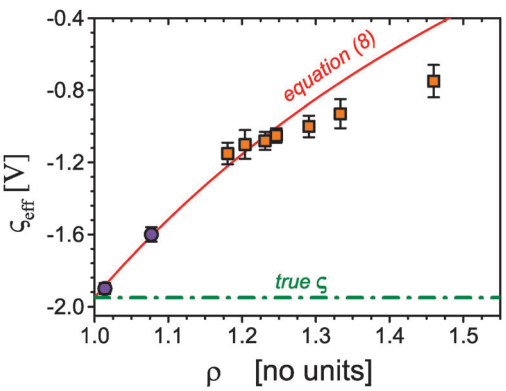

Fig. 8 Variation of effective electrocapillary coupling coefficient, ς_{eff}, with surface roughness factor, ρ. Circles and squares show experimental data from the annealing (circles) and the relaxation (squares) experiments are compared to the prediction of eqn (9) (red line). The true value, ς, of the coupling parameter was set to −1.95 V. Note the good agreement between theory and experiment in the range of validity of eqn (9), that is, for small roughness.

V. Conclusion

This study documents, from the points of view of theory and of experiment, the significant impact of surface roughness on the effective value of the electrocapillary coupling coefficient ς_{eff}. Starting out from previously published results from surface mechanics we derive a correction scheme that requires, as the appropriate surface morphology parameter, knowledge of the roughness factor, that is, the ratio of true over projected area of electrode. As exemplified in our study, the roughness factor is readily measured, for instance by analysis of surface height profiles measured by atomic force microscopy, or from capacitance ratio data. By studying the electrocapillary coupling on surfaces with different roughness we have shown that (i), roughness even on nominally planar surfaces can induce substantial error in experimental data for the electrocapillary coupling, and (ii) that our analysis achieves a precise correction provided that the roughness is not too large.

As our study illustrates, the correction scheme may be conveniently applied to experimental studies of surface stress and of electrocapillary coupling. We therefore suggest it's routine application in future studies, anticipating a significantly enhanced accuracy.

Acknowledgements

Support by China Scholarship Council (Q. Deng) and by Deutsche Forschungsgemeinschaft (grant WE 1424/16) is gratefully acknowledged.

References

1 H. Ibach, *Surf. Sci. Rep.*, 1997, **29**, 193.
2 H. Ibach, *Physics of Surfaces and Interfaces*, Springer, 2006, pp. 1–643.
3 S. A. Akhade and J. R. Kitchin, *J. Chem. Phys.*, 2012, **137**, 084703.
4 W. Haiss, R. J. Nichols, J. K. Sass and K. P. Charle, *J. Electroanal. Chem.*, 1998, **452**, 199.
5 W. Haiss, *Rep. Prog. Phys.*, 2001, **64**, 591.
6 A. Ruban, B. Hammer, P. Stoltze, H. L. Skriver and J. K. Nrskov, *J. Mol. Catal. A: Chem.*, 1997, **115**, 421.
7 V. I. Levitas, V. F. Nesterenko and M. A. Meyer, *Acta Mater.*, 1998, **46**, 5929.
8 M. Mavrakakis, B. Hammar and J. K. Nrskov, *Phys. Rev. Lett.*, 1998, **81**, 2819.
9 P. Dolle, R. Baudoing-Savois, M. De Santis, M. C. Saint-Lager, M. Abel, J. C. Bertolini and P. Delichère, *Surf. Sci.*, 2002, **518**, 1.

10 L. A. Kibler, A. M. El-Aziz and D. M. Kolb, *J. Mol. Catal. A: Chem.*, 2003, **199**, 57.
11 L. A. Kibler, A. M. El-Aziz, R. Hoyer and D. M. Kolb, *Angew. Chem., Int. Ed.*, 2005, **44**, 2080.
12 P. Strasser, S. Koh, T. Anniyev, J. Greeley, K. More, C. Yu, Z. Liu, S. Kaya, D. Nordlund, H. Ogasawara, M. F. Toney and A. Nilsson, *Nat. Chem.*, 2010, **2**, 454.
13 J. Weissmüller, R. N. Viswanath, L. A. Kibler and D. M. Kolb, *Phys. Chem. Chem. Phys.*, 2011, **13**, 2114.
14 Q. Deng, M. Smetanin and J. Weissmüller, *J. Catal.*, 2014, **309**, 351.
15 Q. Deng and J. Weissmüller, *Langmuir*, 2014, **30**, 10522.
16 J. Weissmüller, in *Electrocatalysis: Theoretical Foundations and Model Experiments*, ed. R. C. Alkire, L. Kibler, D. M. Kolb and J. Lipkowski, Electrocapillarity of Solids and its Impact on Heterogeneous Catalysis, Wiley VCH, Weinheim, Germany, 2013, pp. 163–220.
17 A. Ya. Gokhshtein, *Dokl. Akad. Nauk SSSR*, 1969, **187**, 601.
18 J. Weissmüller and D. Kramer, *Langmuir*, 2005, **21**, 4592.
19 M. Smetanin, R. N. Viswanath, D. Kramer, D. Beckmann, T. Koch, L. A. Kibler, D. M. Kolb and J. Weissmüller, *Langmuir*, 2008, **24**, 8561.
20 M. C. Lafouresse, U. Bertocci, C. R. Beauchamp and G. R. Stafford, *J. Electrochem. Soc.*, 2012, **159**, H816.
21 M. C. Lafouresse, U. Bertocci and G. R. Stafford, *J. Electrochem. Soc.*, 2013, **160**, H636.
22 R. N. Viswanath, D. Kramer and J. Weissmüller, *Electrochim. Acta*, 2008, **53**, 2757.
23 H. J. Jin, S. Parida, D. Kramer and J. Weissmüller, *Surf. Sci.*, 2008, **602**, 3588–3594.
24 H. J. Jin, X. L. Wang, S. Parida, K. Wang, M. Seo and J. Weissmüller, *Nano Lett.*, 2010, **10**, 187.
25 M. Smetanin, Q. Deng and J. Weissmüller, *Phys. Chem. Chem. Phys.*, 2011, **13**, 17313.
26 J. Fritz, M. K. Baller, H. P. Lang, H. Rothuizen, P. Vettiger, E. Meyer, H. J. Guntherodt, C. Gerber and J. K. Gimzewski, *Science*, 2000, **288**, 316.
27 J. J. Headrick, M. J. Sepaniak, N. V. Lavrik and P. G. Datskos, *Ultramicroscopy*, 2003, **97**, 417.
28 N. V. Lavrik, C. A. Tipple, M. J. Sepaniak and P. G. Datskos, *Chem. Phys. Lett.*, 2001, **336**, 371.
29 A. G. Hansen, M. W. Mortensen, J. E. T. Andersen, J. Ulstrup, A. Kuhle, J. Garnæs and A. Boisen, *Probe Microsc.*, 2001, **2**, 139.
30 R. Desikan, I. Lee and T. Thundat, *Ultramicroscopy*, 2006, **106**, 795.
31 V. Tabard-Cossa, M. Godin, I. J. Burgess, T. Monga, R. B. Lennox and P. Grutter, *Anal. Chem.*, 2007, **79**, 8136.
32 J. Weissmüller and H. Duan, *Phys. Rev. Lett.*, 2008, **101**, 146102.
33 Y. Wang, J. Weissmüller and H. Duan, *J. Mech. Phys. Solids*, 2010, **58**, 1552.
34 M. E. Gurtin, J. Weissmüller and F. Larché, *Philos. Mag. A*, 1998, **78**, 1093.
35 B. Özkaya, S. R. Saranu, S. Mohanan and U. Herr, *Phys. Status Solidi A*, 2008, **205**, 1876.
36 S. Djaziri, D. Faurie, E. Le Bourhis, P. Goudeau, P.-O. Renault, C. Mocuta, D. Thiaudiére and F. Hild, *Thin Solid Films*, 2013, **530**, 30.
37 H. Angerstein-Kozlowska, B. E. Conway, A. Hamelin and L. Stoicoviciu, *Electrochim. Acta*, 1986, **31**, 1051.
38 H. Angerstein-Kozlowska, B. E. Conway, A. Hamelin and L. Stoicoviciu, *J. Electroanal. Chem.*, 1987, **228**, 429.
39 F. El Feninat, *et al.*, *Appl. Surf. Sci.*, 2001, **183**, 205.
40 C. Y. Poon and B. Bhushan, *Wear*, 1995, **190**, 76.
41 Y. Umeno, C. Elsässer, B. Meyer, P. Gumbsch, M. Nothacker, J. Weissmüller and F. Evers, *Europhys. Lett.*, 2007, **78**, 13001.
42 J.-M. Albina, C. Elsässer, J. Weissmüller, P. Gumbsch and Y. Umeno, *Phys. Rev. B: Condens. Matter Mater. Phys.*, 2012, **85**, 125118.
43 S. Trasatti and A. Petrii, *Pure Appl. Chem.*, 1991, **63**, 711.
44 D. Faurie, P.-O. Renault, E. Le Bourhis, P. Villain, P. Goudeau and F. Badawi, *Thin Solid Films*, 2004, **469–470**, 201.
45 D. J. Trevor, C. E. D. Chidsey and D. N. Loiacano, *Phys. Rev. Lett.*, 1989, **62**, 929.
46 M. A. Schneeweiss and D. M. Kolb, *Solid State Ionics*, 1997, **94**, 171.
47 C. Alonso, R. C. Salvarezza, J. M. Vara and A. J. Arvia, *J. Electrochem. Soc.*, 1990, **137**, 2161.
48 M. P. Garcá, M. M. Gómez, R. C. Salvarezza and A. J. Arvia, *J. Electrochem. Soc.*, 1994, **141**, 2291.
49 G. Andreasen, M. Nazzarro, J. Ramirez, R. C. Salvarezza and A. J. Arvia, *J. Electrochem. Soc.*, 1996, **143**, 466.